Microelectronics Reliability 51 (2011) 1385–1392

Contents lists available at ScienceDirect

Microelectronics Reliability

journal homepage: www.elsevier.com/locate/microrel

Characterization of elasto-plastic behavior of actual SAC solder joints for drop test modeling

Tung T. Nguyen, Seungbae Park *

Department of Mechanical Engineering, State University of New York at Binghamton, Binghamton, NY 13902, United States

ARTICLE INFO

Article history:
Received 30 December 2010
Received in revised form 27 February 2011
Accepted 2 March 2011
Available online 6 April 2011

ABSTRACT

This paper focuses on the characterization of the elasto-plastic properties of actual Sn–1.0 wt.%Ag–0.5 wt.%Cu (SAC105), Sn–3.0 wt.%Ag–0.5 wt.%Cu (SAC305) and Sn–4.0 wt.%Ag–0.5 wt.%Cu (SAC405) solder joints for drop test modeling. Several actual ChipArray® BGA (CABGA) packages were cross-sectioned, polished and used as the test vehicles. The drop tests were performed with various impact amplitudes using a specially designed mini drop table along with a conventional drop table to generate plastic deformations in the solder joints. The plastic deformations in the solder joints were measured after each drop using microscope imaging in conjunction with the digital image correlation (DIC) technique. The coefficients of the Ramberg–Osgood elasto-plastic model for the solder alloys were extracted from the experimental results using a finite element method (FEM) modeling-based iteration process. An application and validation of the developed model were carried out using pendulum tests.

1. Introduction

Board level solder joint reliability during drop impact is a great concern in electronic packaging. A widely accepted method to assess the drop reliability of microelectronics is the drop test [1]. Modeling is also a powerful method which can provide insight into the dynamic behaviors of the BGA packages under drop impact [2,3]. Moreover, modeling is usually used to compare the relative drop test performance of various package designs. Since solder alloys deform plastically at high stress and high strain rate, the elasto-plastic properties of the solder alloys are needed to support the drop test modeling. Therefore, it is important to characterize the elasto-plastic properties accurately in order to achieve a reliable drop test model.

A number of studies have been reported on the characterization of elasto-plastic properties of lead and lead-free solder alloys. Darveaux and Banerji [4] developed constitutive relations for tin-based solder joints using tensile and shear tests. Wang and Yi [5] reported compressive constitutive properties of 63Sn37Pb solder over the strain rates from 340 to 1150 s^{-1} using split Hopkinson pressure bar (SHPB) test. Vianco et al. [6] characterized the time-independent mechanical and physical properties of the ternary 95.5Sn3.9Ag0.6Cu solder over the temperature range of −25 to 160 °C using strain rates of 4.2×10^{-5}–8.3×10^{-4}. Siviour et al. [7] measured bulk properties of Sn37Pb, Sn3.5Ag, and Sn3.8Ag0.7-Cu using SHPB at strain rates from 500 to 3000 s^{-1}. Wiese and Rzepka [8] investigated time-independent behavior of SnPb37, SnAg3.5, and SnAg4Cu0.5 on flip chip solder joints using a micro shear tester. Wong et al. [9] generated true stress strain properties of four solder alloys (63Sn–37Pb, Sn1.0Ag0.1Cu, Sn–3.5Ag, and Sn3.0Ag0.5Cu) for strain rates in the range from 0.005 s^{-1} to 300 s^{-1} using a specialized drop-weight tester. Jenq et al. [10] studied compression behavior of SAC305, SAC105, and Sn–37Pb at strain rates ranging from 380 to 3030 s^{-1} using the SHPB apparatus. Qin et al. [11] investigated mechanical properties of one lead-based solder, Sn37Pb, and two lead-free solders, Sn3.5Ag and Sn3.0Ag0.5Cu at strain rates that ranged from 600 s^{-1} to 2200 s^{-1} by the SHPB and tensile bar technique. Based on the experimental data, the strain rate-dependent Johnson–Cook models for the three solders were derived. More recently, Su et al. [12] performed bulk solder tensile tests to characterize the mechanical properties of SAC105 and SAC405 at strain rates ranging from 0.0088 s^{-1} to 57.0 s^{-1}. The authors also conducted solder joint array shear and tensile tests on wafer-level chip scale package (WLCSP) specimens under two test rates of 0.5 mm/s (2.27 s^{-1}) and 5 mm/s (22.73 s^{-1}) to investigate the strength and failure modes of the solder joints. Most of the above investigations used bulk solder bars as the test vehicles. However, the material properties of the small solder joints used in electronics assembly are different from those of bulk solder bars, because they have significantly different microstructures and different intermetallic compound layers. To account for the effects of the microstructures and intermetallic compound distribution, it is necessary to perform the characterization on the actual solder joints. Among the above studies, authors in [4,8,12] performed their material characterizations on miniature solder joints. However, the tests were carried out only at low strain rates, while electronic solder joints usually experience medium

* Corresponding author. Tel.: +1 607 777 3415.
E-mail address: sbpark@binghamton.edu (S. Park).

0026-2714/$ - see front matter © 2011 Elsevier Ltd. All rights reserved.
doi:10.1016/j.microrel.2011.03.019

strain rates during drop impacts [9]; the elasto-plastic properties of actual BGA solder joints at medium strain rates are still unavailable for drop test modeling.

In this paper, time-independent elasto-plastic properties of three solder alloys of current industrial interest, SAC105, SAC305 and SAC405, were characterized on actual BGA solder joints at medium strain rates. While the properties of Sn are known to be anisotropic [13], this work is done to examine how properties of the solder alloys can be characterized with an isotropic assumption that is desirable for simplifying engineering design. The measurement on the actual solder joints at medium strain rates was achieved by using a novel methodology. The methodology is the combination of actual drop test, microscope imaging with DIC, and FEM modeling. DIC is an excellent full-field optical deformation measurement technique. It is widely used to assess in-plane and out-of-plane displacement and strain fields on object surfaces with subpixel accuracy [14,15]. The plastic deformations in the solder joints were directly measured, and thus, no separation of elastic and plastic deformations from the experimental data was needed. The Ramberg–Osgood model was chosen to describe the elasto-plastic behavior of the solder alloys. The Ramberg–Osgood model was created to describe the non-linear relationship between stress and strain in materials near their yield points [16]. It is especially useful for metals that harden with plastic deformation, showing a smooth elastic–plastic transition. Based on the experimental data, the coefficients of the constitutive model were accurately evaluated using an iteration process. A novel test setup was designed for characterizing the deformation of actual solder joints subjected to pendulum tests. DIC technique was successfully combined with the pendulum tests for the validation of the developed model.

2. Experiment

2.1. Test vehicle

The test vehicles are Amkor's CABGA test packages with a 10×10 BGA. The package consists of a 1 mm PCB, 10×10 BGA, 220 μm substrate, 250 μm dummy die, and 600 μm overmold. Three BGA solder alloys, SAC105, SAC305 and SAC405, were investigated. The solder joint height, diameter and pitch are 300, 530, and 800 μm, respectively, while the copper pad and polyimide passivation have a thickness of 25 μm. The solder joints were naturally aged at room temperature for several months in order to bring the microstructure closer to an equilibrium state. The packages were then cross-sectioned into samples containing 3×2 solder joints, where each solder joint in the first and the third rows contain only half a solder joint, as shown in Fig. 1. The samples were manually ground and polished using 320–1200 grit silicon carbide papers to be ready for the tests. For the solder alloys used in this study the cross-sectioned surfaces of the solder joints were found to have sufficiently detailed contrast features on the surfaces (see Fig. 1d to allow local displacement changes to be measured using DIC calculations, making any further surface treatment unnecessary.

2.2. Experimental setup

Fig. 2 shows the schematic of the drop test setup. The test sample was mounted on a mini drop table, which was designed and made of aluminum. It consists of a base plate, a drop weight and two parallel rods to guide the drop weight. Two springs were also used to press the drop weight onto the test sample, and thus, to ensure the test sample is in contact with the drop weight and the base before the drop table hits the strike surface. The springs were chosen to have a low enough stiffness, so that they have negligible effect on deformation of the test sample. The mini drop table was then mounted to the top of a conventional drop table using four screws, one at each corner of the base plate. When the drop table is dropped the drop weight will generate compressive force on the test vehicle during the impact, inducing deformation in the solder joints. This technique is fundamentally similar to the drop weight technique used in [9]. The difference between them is that in this technique the test vehicle is dropped along with the drop weight instead of staying fixed on the bottom base. This way was found to help produce more uniform deformation distribution among the solder joints in the test sample. During the drop tests, an accelerometer was placed on the top corner of the base of the mini drop table to monitor the transient acceleration of the base. It is noted that the acceleration profile was observed to have a typical half-sine pulse shape as shown in Fig. 2b.

Consecutive drops were performed at peak accelerations from 400 G to 3000 G, with 200 G increments after each drop. The drop height was adjusted to get the desired peak accelerations. Stress–strain behavior of solder alloys is known as rate-dependent. It is desirable to conduct the material characterization at constant strain rates. However, the strain distribution in the solder joint is non-uniform, because of its irregular geometry. Therefore, it is not as possible to generate uniform strain rates in the actual solder joints as it is in a bulk solder bar with a uniform cross-section. In this study, the impact duration was adjusted to be 0.5 ms in an attempt to be in the strain rate range of the practical board level drop tests suggested by JEDEC [1]. Since the maximum strain observed in the experiments is around 2.5%, the maximum strain rate can be approximately estimated as $100\ s^{-1}$. This strain rate is in a similar range estimated for mobile applications by authors in [9]. A photograph of the experimental setup is shown in Fig. 3.

After each drop, the 8-bit gray level images of the cross-sectioned surfaces of the solder joints were magnified with a microscope and recorded with the CCD camera. The surfaces were magnified by using a 20× objective lens, by which a field-of-view size of approximately $522 \times 697\ \mu m^2$ was obtained. For this setup the error of the displacement measurement is estimated to be ±0.002 μm [15]. The recorded images were correlated with the reference ones taken before the drop tests to obtain the residual displacement and strain fields in the solder joints. The displacement fields were obtained for four cross-sectioned solder joints from 1 to 4 (see Fig. 1b). The final displacement of each sample is the mean value of the four solder joints.

2.3. Experimental results

The DIC was performed using the acquired images; the displacement fields in *x*-direction and *y*-direction were obtained. However, only displacement in *y*-direction was used for the extraction of the coefficients for the constitutive model. A typical set of results from DIC is shown in Fig. 4. The contour plot in Fig. 4a depicts well the behaviors of the solder joint under compression. Locations 0 and 1 designate areas on the top and bottom of the solder joints, respectively, as indicated in Fig. 4a. Since the experimentally obtained distributions are not uniform in these locations, displacement *Y* was averaged in locations 0 and 1. Then, the differences between the averaged values of these locations was denoted as the total displacements in *Y* of the solder joint, respectively, in the rest of the paper. Finally, the displacement, *Y*, of a test sample is the mean value of the four cross-sectioned solder joints of the sample (see Fig. 1b). It is noted that the measured displacements are residuals after load is removed, which contain only the plastic components, and thus, no separation of elastic and plastic displacements is needed.

Fig. 5 shows the resultant plastic displacement *Y* versus acceleration peak. It is noted that each data point in the figure is the mean

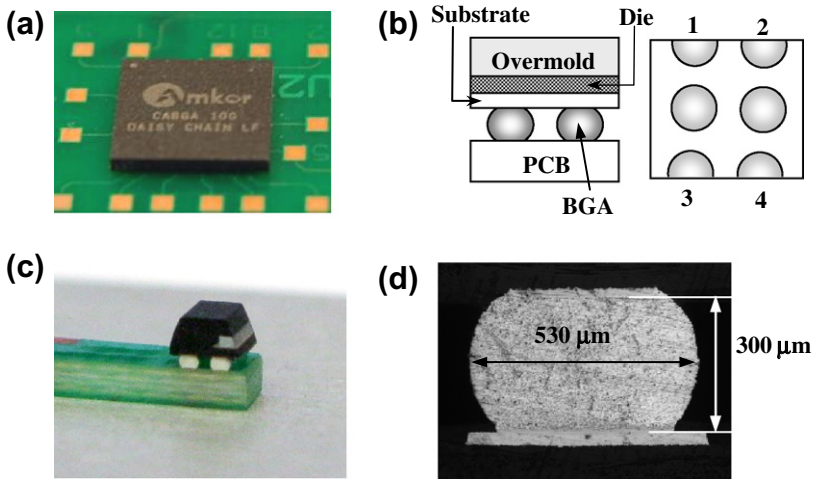

Fig. 1. Test vehicle (a) CABGA package, (b) schematics of the cross-sectioned sample, (c) picture of the cross-sectioned sample, (d) polished surface of the solder joint.

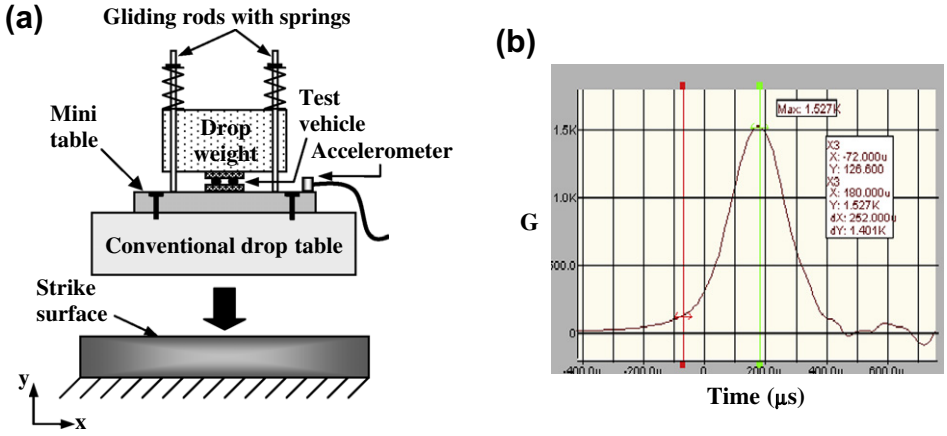

Fig. 2. (a) Schematic of the pulse-controlled drop test. (b) A typical half-sine pulse shape observed from the drop test.

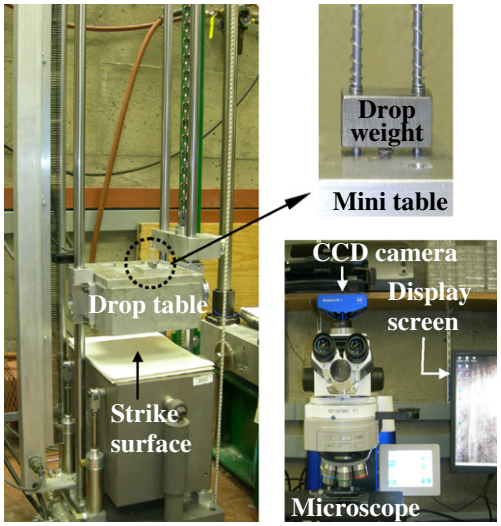

Fig. 3. Experimental setup for the drop tests.

value of six different test samples of four cross-sectioned solder joints. Curve fitting was performed to fit the experimental data. The details of the curve fitting will be discussed later in Section 3.3.

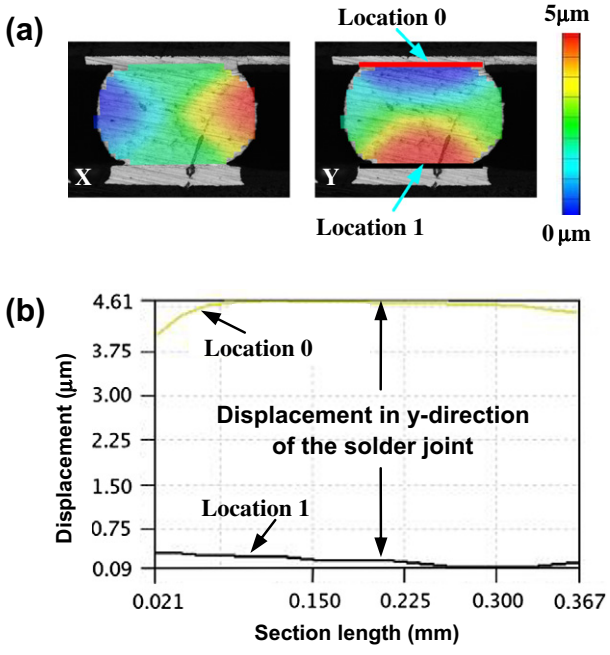

Fig. 4. A typical set of results from DIC (a) contour plot of plastic displacements in *x* and *y*-directions, (b) plastic displacements in *y*-direction in the created locations.

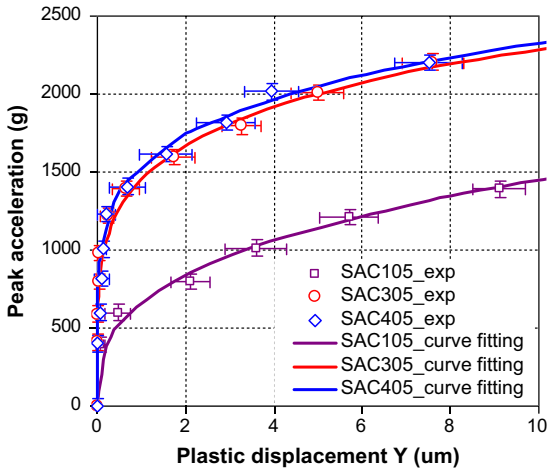

Fig. 5. Plastic displacement Y versus acceleration peak.

3. Extraction of the coefficients for the elasto-plastic models

3.1. FEM modeling

Since the geometry of the solder joint is not regular the stress and strain distributions during the experiment could not be obtained by simple analytical calculations. Therefore, drop test modeling was performed for the extraction of the elasto-plastic properties of the solder alloys. The 3D FEM model was constructed as shown in detail in Fig. 6. The model consists of the test vehicle and the drop weight. The geometries, materials, boundary condition, loads were set to the same as those in the experiments. Thus, the bottom of the PCB was constrained in y-direction; a contact pair was defined between the top of the overmold and the bottom of the drop weight. The transient analyses were performed with ANSYS using "Input-G" method and the implicit solver [3]. The transient accelerations recorded with the accelerometer from the experiments were applied to the FEM model as the loading. The damping ratio is arbitrarily assumed to be 2%.

3.2. Constitutive model

All the constitutive materials were modeled as linear elastic materials except for the solder alloys which were modeled as time-independent elasto-plastic materials. The elastic properties of the constitutive materials were obtained from [15]. Ramberg–Osgood model was chosen for the solder alloys. The model was successfully used by the authors in [17] to describe the elasto-plastic behavior of several solder alloys. The original form of the model can be written as

$$\varepsilon = \frac{\sigma}{E} + K\left(\frac{\sigma}{E}\right)^n \tag{1}$$

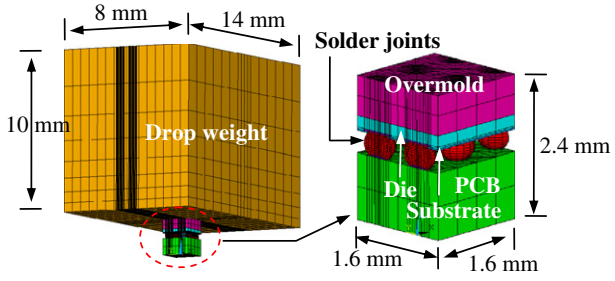

Fig. 6. 3D FEM model for the drop tests.

where ε is strain, σ is stress, E is Young's modulus, n is the hardening exponent and K is a material constant. The first term of the equation σ/E is equal to the elastic part of the strain, while the second term, $K(\sigma/E)^n$, accounts for the plastic part; the parameters K and n describe the hardening behavior of the material. The Ramberg–Osgood equation can be rewritten as

$$\varepsilon = \frac{\sigma}{E} + \left(\frac{\sigma}{\sigma_0}\right)^n \tag{2}$$

where $\sigma_0 = E/K^{1/n}$. The coefficients of the model $\{n, \sigma_0\}$ now need to be extracted from the experimental data. The determination of the coefficients of the model will be discussed in the next section.

3.3. Iteration process

Since the Ramberg–Osgood stress–plastic strain relationship is a power law relation, it is also employed to describe the relationship between the plastic displacement Y_{plas} and peak acceleration g as follows:

$$Y_{plas} = \left(\frac{g}{g_0}\right)^m \tag{3}$$

By fitting the experimental data $\{g, Y_{plas}\}$ into Eq. (3) material constants $\{m, g_0\}$ for SAC105, SAC305 and SAC405 were found to be {2.96, 664.8}, {5.1, 1458} and {5.6, 1539}, respectively (see Fig. 5). Let these be $\{M, G_0\}$'s, the reference values of $\{m, g_0\}$. Based on these results, $\{n, \sigma_0\}$ for the solder alloys are needed to be determined so that the drop test modeling would produce the same $\{g, Y_{plas}\}$ relationship as the experiments do. In other words, the above reference values of $\{m, g_0\}$ should be also obtained when fitting the numerically-obtained values of $\{g, Y_{plas}\}$ into Eq. (3). Since $\{n, \sigma_0\}$ could not be determined explicitly, an iteration process was developed as shown in Fig. 7. The process begins with estimated initial values of $\{n, \sigma_0\}$ as the input. Now that $\{n, \sigma_0\}$ are known 20 stress–strain points, of which the values of stress ranging from 10 to 200 MPa (with 10 MPa distance from one to the next), are derived from Eq. (2) and used as the inputs for the multilinear kinematic hardening model (*TB, KINH*) in ANSYS [18]. In this way the Ramberg–Osgood model is conveniently adopted into ANSYS. The drop test modeling is then performed at the peak accelerations ranging from 400 G to 3000 G. The plastic displacements Y_{plas} in the solder joints are obtained from the results of the modeling. Curve fitting is

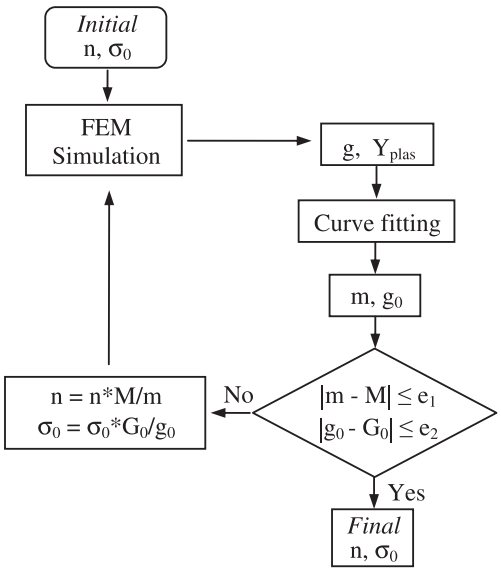

Fig. 7. Iteration process for the extraction of $\{n, \sigma_0\}$.

performed to fit the numerically-obtained data $\{g, Y_{plas}\}$ into Eq. (3) to obtain the coefficients $\{m, g_0\}$. If these coefficients are close enough to their above reference values $\{M, G_0\}$, the iteration process is terminated. Otherwise, a new set of $\{n, \sigma_0\}$ is calculated (see Fig. 7); and the iteration is repeated until convergence is achieved. The values for convergence criteria e_1 and e_2 were set to be $10^{-3}M$ and $10^{-3}G_0$, respectively, in this paper.

4. Results and discussions

Generally, the solution was found to converge after less than six iterations with reasonable initial values of $\{n, \sigma_0\}$. The final values of $\{n, \sigma_0\}$ for SAC105, SAC305 and SAC405 were found to be {3.1, 213}, {5.4, 232} and {6, 215}, respectively. The hardening exponents n for SAC305 and SAC405, 5.4 and 6 respectively, are marginally smaller than the literature values for 95.5Sn3.8Ag0.7Cu solder bar which range from 7.96 to 9.41 [17]. The Ramberg–Osgood equations for SAC105, SAC305 and SAC405, can then be respectively written as

$$\varepsilon_{SAC105} = \frac{\sigma}{97} + \left(\frac{\sigma}{213}\right)^{3.1} \quad (4)$$

$$\varepsilon_{SAC305} = \frac{\sigma}{90} + \left(\frac{\sigma}{232}\right)^{5.4} \quad (5)$$

$$\varepsilon_{SAC405} = \frac{\sigma}{86} + \left(\frac{\sigma}{215}\right)^{6} \quad (6)$$

The unit of σ in these equations is GPa. The elasto-plastic curves for the solder alloys are shown in Fig. 8. The elasto-plastic curves for SAC405 from Weise [8], SAC101 and SAC305 at strain rate of 100 s^{-1} from Wong [9], SAC305 at strain rate of 600 s^{-1} from Qin et al. [11] are also plotted in the figure for the comparison. It can be observed from the figure that the curves obtained from this paper are generally in good agreement with the ones from literature. The curve for SAC405 in this paper matches every well with Weise and Rzepka's [8], a widely used model for drop test modeling, at strains below 0.015. At higher strains, the Weise's curve exhibits much higher hardening. The elasto-plastic curves for SAC305 and SAC405 obtained from this paper are very close to each other, implying that SAC305 and SAC405 have similar elasto-plastic behavior. Moreover, at the same strain value the stress value for SAC105 is significantly lower than those for SAC305 and SAC405. This indicates that SAC105 is more ductile than SAC305 and SAC405. This result is in agreement with the literature finding that SAC105 solder joints have better reliability than the SAC305 and SAC405 under drop impact [19,20].

Using the models given in Eqs. (4)–(6), the Y_{plas}–g curves for the solder alloys obtained from the drop test modeling are now identical to the best fit curves in Fig. 5. It seen from the figure that the numerical results fit the experimental ones very well. Moreover, the typical contour plots of the plastic displacements X and Y, obtained from the drop test modeling and shown in Fig. 9, match very well with the contour plots of the experimental ones shown in Fig. 4a. Furthermore, when the typical contour plots of strains in x- and y-direction are obtained from the both experiments and modeling, as shown in Fig. 10, the experimental and numerical contour plots also match very well. These results confirm that the choice of Ramberg–Osgood model to describe the elasto-plastic behavior of the solder alloys was proper, and that the coefficients of the model were extracted accurately.

5. An application and validation of the model

In order to validate the developed model high speed pendulum tests were setup and performed. The test vehicle is an Amkor's CTBGA package with 228 solder balls made of SAC405 (see Fig. 11a). The package consists of a 600 μm PCB, 200 μm substrate, 200 μm dummy die, and 600 μm thick over mold. The solder ball height is 230 μm, while the solder ball diameter is 340 μm. It is noted that this solder ball size is smaller than the one used for the material characterization described above. The packages were then cross-sectioned into samples containing 3 × 4 solder joints as shown in Fig. 11b–d. The samples were manually ground and

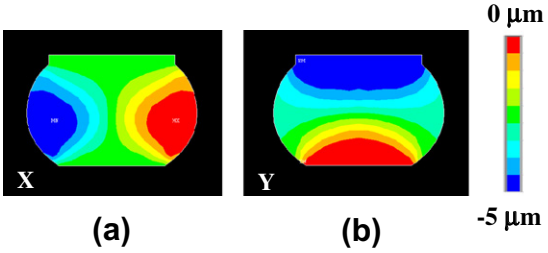

Fig. 9. Typical contour plot of plastic displacements (a) X and (b) Y in the solder joints obtained from drop test modeling.

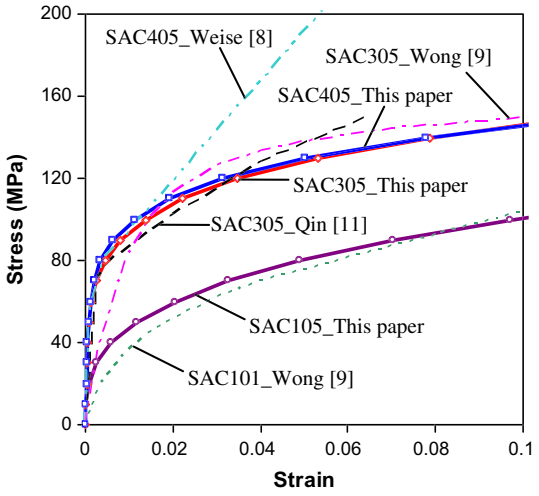

Fig. 8. Comparison of elasto-plastic curves for the solder alloys.

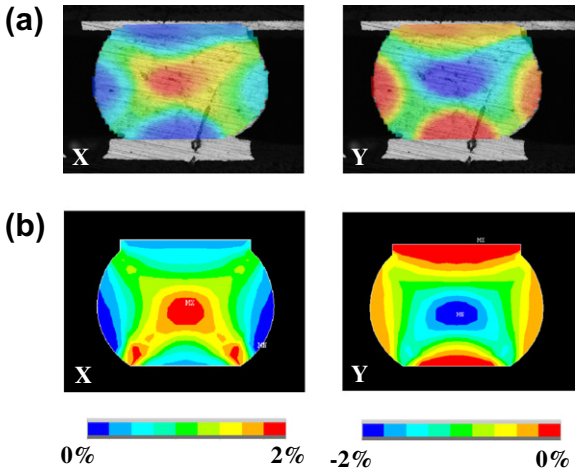

Fig. 10. Typical contour plot of plastic strains X and Y in the solder joints (a) experimental (b) numerical results.

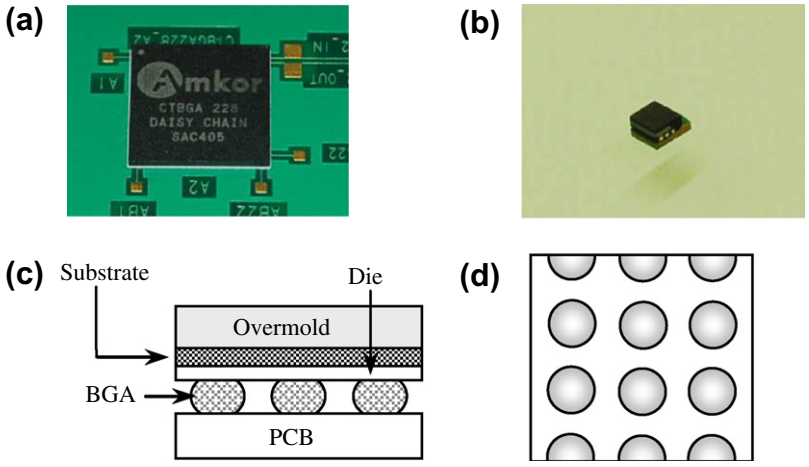

Fig. 11. Test vehicle for the pendulum test (a) Amkor's CTBGA package (b) picture of cross-sectioned sample (c) front view of the schematic of the test sample (d) top view of the schematic of the test sample.

polished using the process described in Section 2.1 to be ready for the tests.

High speed pendulum impact tests were carried out on XYZTEC Condor Impact Measurement Unit. This unit was selected because it has the capability to perform high speed impact tests [21]. The schematic of the pendulum test is shown in Fig. 12. The test vehicle was glued, using epoxy, onto an aluminum base which was rigidly constrained. The pendulum was controlled to impact the substrate and molding compound layers in horizontal direction, inducing shear deformations in the solder joints. A shear height of 230 μm from the PCB surface was adopted for all the tests. This shear height was selected to make sure the pendulum head would hit the top part of the test sample including the molding compound, die and substrate. The pendulum head was programmed to swing with a constant speed, then, hit and knock off the top part of the test vehicle. The speed was selected to be 0.4 m/s so that the impact duration was approximately 1 ms, which is similar to the one in the above drop tests. The transducer in the equipment captured impact force data as a function of time. A picture of the experimental setup is shown in Fig. 13.

Two identical samples were prepared and tested. The failure mode observed from the tests was crack in the intermetallic layer formed between the bulk solder and the copper pad at the PCB side. After the pendulum test the displacement fields in all the cross-sectioned solder joints were obtained using the DIC process as described in the previous sections. A typical contour plot of the displacement *X* obtained from the DIC is shown in Fig. 14. The shear displacement between the top and the bottom of all the cross-sectioned solder joints was found to be average of 19.7 μm.

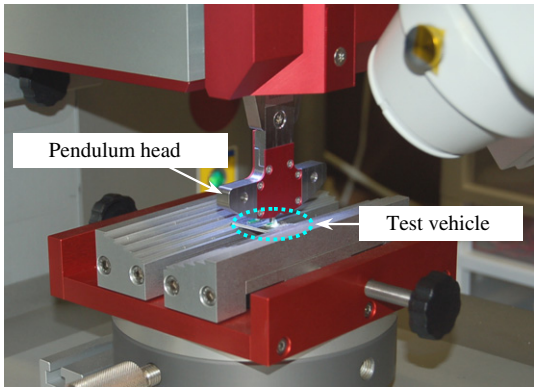

Fig. 13. A picture of the high speed pendulum test setup.

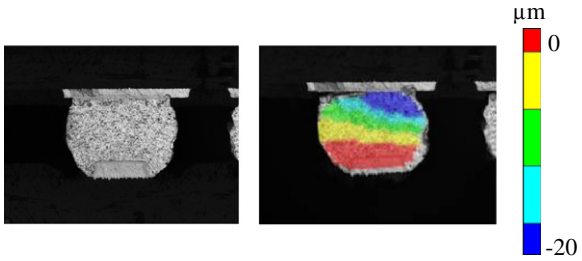

Fig. 14. Contour plot of displacement *X* (a) before the test (b) after the test.

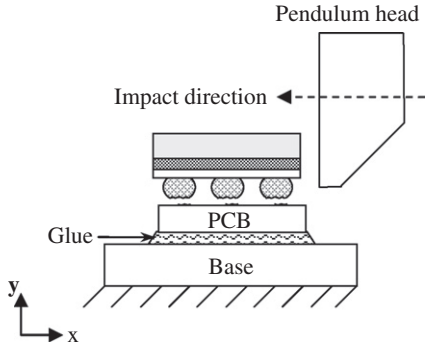

Fig. 12. Schematic of the high speed pendulum test.

The reaction force recorded by the transducer is shown in Fig. 15. Generally, the reaction force increases sharply as the pendulum impacts the sample. It reaches its highest value, when the crack begins in the intermetallic layer, and then decreases to zero. In both of the tests, the peak reaction force was approximately 29.5 N.

Transient FEM modeling was conducted to simulate the pendulum tests. The 3D FEM model of the pendulum test is shown in Fig. 16. The bottom of the PCB was constrained in all DOF's. The reaction force experimentally recorded was uniformly applied to the composite of the molding compound, die and substrate layers

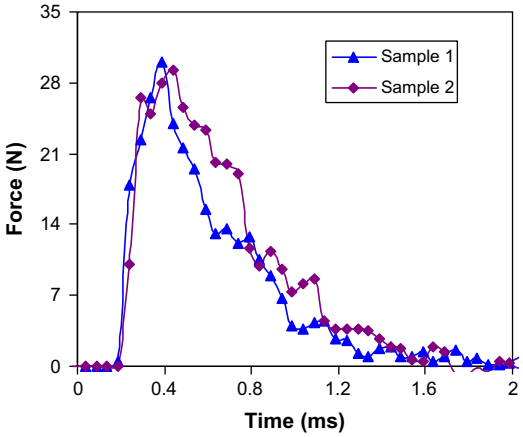

Fig. 15. Transient reaction force at the pendulum head.

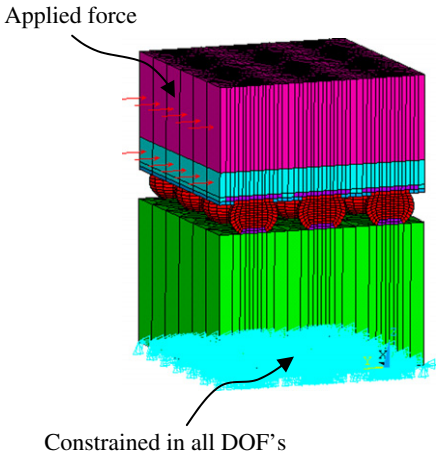

Fig. 16. 3D FEM model of the pendulum test.

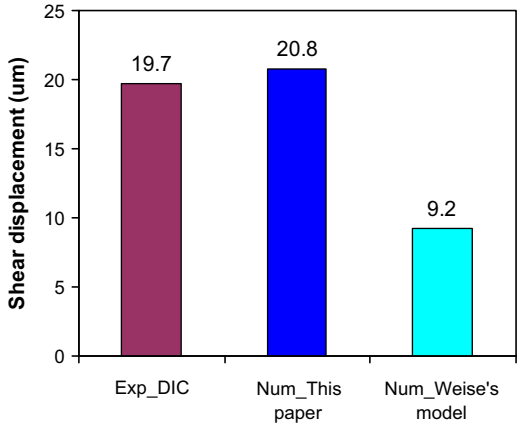

Fig. 17. Comparison of the experimental and numerical results for the shear displacement in the solder joints after the pendulum test.

of the model as the transient loading. The developed constitutive equation for SAC405 (Eq. (6)) was applied for the solder joints. It is assumed that the cracks happen when the reaction force reaches its peak value. During the crack openings, the reaction force decreases; the plastic deformation in the solder joints remains the same. Therefore, in the FEM simulation, fracture of the solder joints was not considered.

For the comparison purpose, Weise's elasto–plastic model [8] was also used in the simulation. Weise's model was chosen because it is considered the most widely used model for drop test modeling of electronic packaging recently. The comparison of the experimental results obtained from the pendulum tests, the simulation results with the developed model and Weise's model, respectively, is presented in Fig. 17. It is noted that the DIC result in the figure is the mean value of the 12 cross-sectioned solder joints of the two samples. The figure clearly shows that the model in this paper produces very good match between the experimental and numerical results, while Weise's model underestimates the shear displacement. This result validates the constitutive model developed in this work.

6. Conclusion

The elasto-plastic behaviors of actual SAC105, SAC305 and SAC405 solder joints were characterized at medium strain rates using a novel methodology, in which drop tests were combined with DIC and FEM modeling. The Ramberg–Osgood model was used to describe the elasto-plastic behavior of the solder alloys. The coefficients of the models for the solder alloys were successfully extracted from the experimental results using the developed iteration process. The developed elasto-plastic model produced good agreement between the numerical and experimental results for both drop and pendulum tests. The model is recommended to be used to describe the behaviors of the solder alloys in drop test modeling of electronic packaging.

Acknowledgments

The authors would like to thank all the members of Opto-Mechanics Research Lab, Vibration Lab, and Material Processing Lab at Binghamton University for their helpful support.

References

[1] JEDEC standard: board level drop test method of components for handheld electronic products, JESD22-B111, 2003.
[2] Tsai TY, Lai YS, Yeh CL, Chen RS. Structural design optimization for board-level drop reliability of wafer-level chip-scale packages. Microelectron Reliab 2008;48(5):757–62.
[3] Park SB, Shah C, Kwak J, Jang CS, Pitarresi J. Transient dynamic simulation and full-field test validation for a slim PCB of mobile phone under drop/impact. In: Reno NV, editor. Proceedings of 57th electronic components and technology conference; May 2007. p. 914–23.
[4] Darveaux R, Banerji K. Constitutive relations for tin-based solder joints. IEEE Trans Compon Hybrids Manuf Technol 1992;15(6):1013–24.
[5] Wang B, Yi S. Dynamic plastic behavior of 63Sn37Pb eutectic solder under high strain rates. J Mater Sci Lett 2002;21:697–8.
[6] Vianco PT, Rejent JA, Kilgo AC. Time-independent mechanical and physical properties of the ternary 95.5Sn–3.9Ag–0.6Cu solder. Electron Mater 2003;32(3):142–51.
[7] Siviour CR, Williamson DM, Palmer SJP, Walley SM, Proud WG Field JE. Dynamic properties of solders and solder joints. J Phys IV 2003;110(1):477–82.
[8] Wiese S, Rzepka S. Time-independent elastic–plastic behaviour of solder materials. Microelectron Reliab 2004;44:1893–900.
[9] Wong EH, Selvanayagam CS, Seah SKW, van Driel WD, Caers JFJM, Zhao XJ, et al. Stress–strain characteristics of tin-based solder alloys for drop-impact modeling. J Electron Mater 2008;37(6):829–35.
[10] Jenq ST, Chang HH, Lai YS, Tsai TY. High strain rate compression behavior for Sn–37Pb eutectic alloy, lead-free Sn–1Ag–0.5Cu and Sn–3Ag–0.5Cu alloys. Microelectron Reliab 2009;49:310–7.
[11] Qin F, An T, Chen N. Strain rate effects and rate-dependent constitutive models of lead-based and lead-free solders. Appl Mech 2010;77(1). 011008-1-11.
[12] Su YA, Tan LB, Tee TY, Tan VBC. Rate-dependent properties of Sn–Ag–Cu based lead-free solder joints for WLCSP. Microelectron Reliab 2010;50(4):564–76.
[13] Park SB, Dhakal R, Lehman L, Cotts E. Measurement of deformations in SnAgCu solder interconnects under in situ thermal loading. Acta Mater 2007;55(9):3253–60.
[14] Pan B, Qian K, Xie H, Asundi A. Two-dimensional digital image correlation for in-plane displacement and strain measurement: a review. Meas Sci Technol 2009;20:1–17.

[15] Nguyen TT, Yu D, Park SB. Characterizing the mechanical properties of actual SAC105, SAC305 and SAC405 solder joints by digital image correlation. Electron Mater, in press. doi:10.1007/S11664-011-1534-z.
[16] Ramberg W, Osgood WR. Description of stress–strain curves by three parameters. Technical Note No. 902, National Advisory Committee For Aeronautics, Washington, DC; 1943.
[17] Pang JHL, Xiong BS, Che FX. Modeling stress strain curves for lead-free 95.5Sn–3.8Ag–0.7Cu solder. In: Proceedings of the 5th international conference on thermal and mechanical simulation and experiments in microelectronics and microsystems, Paris, France, October; 2004. p. 449–53.
[18] ANSYS 12 user's manual.
[19] Zhu WH, Xu L, Pang JHL, Zhang XR, Poh E, Sun YF, et al. Drop Reliability study of PBGA assemblies with SAC305, SAC105 and SAC105-Ni solder ball on Cu-OSP and ENIG surface finish. In: Electronic components and technology conference, Lake Buena Vista, FL; May 2008. p. 1667–72.
[20] Suh DW, Kim DW, Liu P, Kim HC, Weninger JA, Kumar CM, et al. Effects of Ag content on fracture resistance of Sn–Ag–Cu lead-free solders under high-strain rate conditions. Mater Sci Eng A 2009:460–1. 595–603..
[21] Pradosh Guruprasad, James Pitarresi, Bob Sykes. Effect of temperature on transition in failure modes for high speed impact test of solder joint and comparison with board level drop test. In: Electronic components and technology conference, Las Vegas, NV; June 2010. p. 908–15.